Applied Energy 259 (2020) 114129

Contents lists available at ScienceDirect

Applied Energy

journal homepage: www.elsevier.com/locate/apenergy

Influence of advanced cylinder coatings on vehicular fuel economy and emissions in piston compression ring conjunction

N. Dolatabadi[a,*], M. Forder[a], N. Morris[a], R. Rahmani[a], H. Rahnejat[a], S. Howell-Smith[a,b]

[a] Wolfson School of Mechanical, Electrical and Manufacturing Engineering, Loughborough University, Leicestershire, UK
[b] Capricorn Automotive Ltd., Basingstoke, UK

HIGHLIGHTS

- A multi-physics, multi-scale model evaluates engine component power loss.
- Effect of advanced coatings on energy efficiency and emissions is evaluated.
- The potential global implications of using advanced coatings is highlighted.

ARTICLE INFO

Keywords:
Piston compression ring
Surface coatings
Fuel economy
Carbon emissions
Internal combustion engines

ABSTRACT

IC engines contribute to global warming through extensive use of fossil fuel energy and emission of combustion by-products. Innovative technologies such as cylinder de-activation (CDA), after-exhaust heat treatment, surface texturing and coatings are proposed to improve fuel economy and reduce emissions of the vehicle fleet. Therefore, study of coating technology through a comprehensive multi-physics analytical model of engine top compression ring is important to ascertain ways of promoting energy savings. This paper presents a multi-scale, multi-physics model of the compression ring-cylinder bore conjunction, using three alternative bore surfaces. The model comprises ring dynamics, contact tribology, heat transfer and gas blow-by. Tribological and thermal properties of advanced coatings, such as Nickel Nanocomposite (NNC) and diamond-like carbon (DLC) are compared with an uncoated steel bore surface as the base line configuration. Such a comprehensive analysis has not hitherto been reported in open literature, particularly with original contributions made through inclusion of salient properties of alternative bore materials for high performance race engines. Power loss and FMEP are evaluated in a dynamometric test, representative of the World-wide harmonised Light vehicles Test Cycle (WLTC). The NNC coating shows promising tribological improvements. The DLC coating is detrimental in terms of frictional power loss and FMEP, although it can effectively improve sealing of the combustion chamber. The differences in power loss of nominated bore surfaces are represented as fuel mass and CO emissions, using theoretical and empirical relations. For the first time the paper shows that advanced coatings can potentially mitigate the adverse environmental impacts of spark ignition (SI) engines, with significant repercussions when applied to the global gasoline-powered vehicle fleet.

1. Introduction

Despite their negative effect upon climate change, relatively inexpensive fossil fuels account for 85% of expended energy sources. Climate change may be effectively mitigated and even reversed if a 60% reduction in harmful emissions is achieved by 2050 [1]. This is a significant challenge as 75% of the automotive market is still projected to rely upon the use of internal combustion (IC) engines, at least up to 2040 [2]. In the meantime, the immediate concern regarding fuel economy and emissions should be effectively addressed. The efficiency of IC engines can be improved through their mechanical design, operating conditions and pertinent properties of the fuel [3–5]. Modern engines undergo larger thermal and mechanical loads because of their high output power-to-light weight ratio components [6]. 4–15% of the fuel energy is consumed in order to overcome friction within a typical four-stroke IC engine [7]. Piston ring-pack accounts for 40–55% of these losses [8]. Combustion heat is dissipated from piston to cylinder bore through the piston compression rings. The sliding friction

* Corresponding author.
E-mail address: N.Dolatabadi@lboro.ac.uk (N. Dolatabadi).

https://doi.org/10.1016/j.apenergy.2019.114129
Received 18 June 2019; Received in revised form 8 October 2019; Accepted 11 November 2019
Available online 21 November 2019

Nomenclature

A	apparent contact area
A_a	contact area of counter face asperities
A_c	cross-sectional area subject to lubricant shear
A_R	reference area of intake valve
A_s	contact area of piston ring seat-groove conjunction
A_v	wetted contact area
b	piston ring face-width
C_D	coefficient of discharge
c_c	specific heat for the bore surface coating
c_{cs}	crankshaft offset
c_p	specific heat of the lubricant
D_v	diameter of the intake valve head
E	Young's modulus of elasticity
E_{in}	available fuel energy
E_{loss}	energy loss
E^*	reduced (effective) modulus of elasticity
F_e	ring tension
F_g	compression ring gas loading
F_t	total ring contact load
f_b	boundary friction
f_f	total friction
f_v	viscous friction
h	lubricant film thickness
h_m	minimum lubricant film thickness
h_t	coefficient of convective heat transfer
I	second area moment of inertia of the ring cross-section
k_c	thermal conductivity of the bore surface coating
k_l	thermal conductivity of the lubricant
k_r	thermal conductivity of the piston ring coating
L_g	compression ring free end-gap
L_v	average intake valve lift
l	connecting rod length
$\dot{m}$	mass flow rate of air-fuel mixture
$\dot{m}_f$	mass flow rate of fuel
$\dot{m}_l$	mass flow rate of the lubricant through the contact conjunction
N	crankshaft angular velocity
n_R	number of revolutions per engine cycle
P_l	power loss
p	generated lubricant pressure
p_g	gas pressure acting on the compression ring
$\dot{Q}$	generated frictional heat
$\dot{Q}_c$	heat flow rate to the coated bore surface
$\dot{Q}_{cv}$	convective lubricant heat flow rate
Q_{LHV}	lower heating value of fuel
$\dot{Q}_p$	heat flow rate through the piston to the compression ring
$\dot{Q}_r$	heat flow rate to the piston ring
R_{bore}	nominal radius of the cylinder bore
R_f	thermal resistance through coated surface asperities
R_l	thermal resistance through the lubricant film
R_v	thermal resistance through the lubricant boundary layer at the contacting surfaces
r	crank radius
S	axial profile of piston ring face-width
S_f	characteristic length
S_{ku}	kurtosis
S_{pc}	arithmetic mean peak curvature
S_{pd}	peak density of asperities per unit area
S_q	root mean square height
S_{sk}	skewness
T_c	surface temperature of the coated bore
T_e	average lubricant temperature
T_{in}	lubricant inlet temperature
T_{out}	Lubricant outlet temperature
T_p	piston temperature
T_r	surface temperature of piston ring
t	time
U	lubricant entrainment velocity
V_d	cylinder swept volume
W_a	load carried by the asperities
W_t	total load carrying capacity
x_p	piston primary displacement

Greek symbols

β	average radius of curvature of asperity peaks
β_o	Reynold's viscosity-temperature coefficient
γ	specific heat ratio
η	lubricant dynamic viscosity
η_a	asperity density per unit area
η_o	reference viscosity of the lubricant
θ	angular displacement of the crankshaft
λ	Stribeck's lubricant film ratio
ξ	pressure coefficient of boundary shear
ρ	lubricant density
ρ_c	density of bore coating
ρ_o	reference density of the lubricant
σ	composite RMS asperity height of contacting surfaces
τ_o	Eyring shear stress
τ_v	viscous shear stress
ϕ	equivalence ratio
ω	angular velocity of the crankshaft

Abbreviations

AFM	atomic force microscopy
AFR	air-fuel ratio
BDC	bottom dead centre
CDA	cylinder deactivation
DI	direct injection
DLC	diamond-like carbon
EHL	elastohydrodynamics
EI	emission index
FMEP	friction mean effective pressure
IC	Internal combustion
LFM	lateral force mode
NNC	Nickel nanocomposite
Nu	Nusselt's number
RMS	root mean square
SI	spark ignition
TDC	top dead centre
TEHL	thermo-elastohydrodynamic lubrication
WLTC	worldwide harmonised light vehicles' test cycle

generates additional heat at these conjunctions [6]. Hence, the study of thermal and tribological inefficiencies at these conjunctions is imperative to subsequently improve upon fuel economy and emissions.

There have been a fair number of experimental and analytical studies of piston ring inefficiencies. Furuhama et al. [9] experimentally mapped the piston and cylinder bore temperatures in a fired engine. Ring conformability can be accurately predicted using the measured temperature gradients between these components [10]. The experimental studies have not been restricted to thermal effects. Frictional power losses of piston rings can be accurately measured using motored

engine dynamometric tests [8]. In such an approach, cylinder pressures are not representative of fired operating conditions. Major design modifications are required to measure frictional losses in fired engines [8]. Analytical models are important tools for the better understanding of multi-physics, multi-scale tribodynamics of piston rings. The primary focus of analytical models has been on lubrication of rigid piston rings [11,12]. Lubrication models have been developed to incorporate flow continuity, lubricant transport with starved conjunctions and mixed regime of lubrication [11,12]. Priest et al [13] studied rigid body dynamics and wear of lubricated piston ring conjunctions. Comparisons between analytical and experimental wear studies indicated that compression rings undergo geometric changes to their profiles after a running-in period. Therefore, measured ring profiles should be utilised in any analytical study. Mishra et al. [14,15] developed a transient thermo-elastohydrodynamic (TEHL) model of the piston compression ring. They concluded that local deformation of contacting surfaces at this conjunction is insignificant, whilst lubricant piezo-viscous effect cannot be neglected. Elastohydrodynamic (EHL) ring models were employed to study the effects of ring asymmetry and bore out-of-roundness on frictional losses [16]. Baker et al. [17] investigated the elastodynamics of flexible rings and its effect on bore conformability and gas blow-by without taking into account the thermal effects. Styles et al. [18] used AFM in lateral force mode, for the first time, to characterise nano-scale frictional performance of actual engine piston ring-bore contact and subsequently used the data in their model. Morris et al. [19] developed a thermal network model to predict contact temperature in the piston ring-cylinder bore conjunction. Their results for rigid piezo-viscous model complied with the findings of Mishra et al. [14]. Their analysis neglected the combustion heat flow from the piston to the rings. They mainly studied the contact temperature variations due to generated sliding frictional heat. They applied their analytical approach to evaluate the effect of cylinder deactivation (CDA) on piston ring frictional losses. Rahmani et al. [20] suggested that fuel consumption and subsequent adverse emissions due to tribological effects can be reduced through optimal control of cylinder bore temperature.

Considering the high efficiency of modern IC engines, further improvements would mainly rely on innovative technologies such as CDA [21], after-exhaust heat treatment [22,23], surface texturing [24,25] and advanced coatings [26]. The combined study of surface texturing and mechanical properties of coatings has been recently suggested in the friction mean effective pressure (FMEP) analysis of gasoline engines [27]. Bore surfaces are honed using crosshatched or plateau honed patterns [28,29]. These patterns have also been implemented on coated cylinder surfaces [24]. Coating technology has been mostly experimentally investigated for IC engine applications under various conditions, covering standard operation, cold starts, hot scuffing and accelerated wear [30,31]. Surface coatings can alter the tribological and thermal behaviour of contacts. They are typically utilised to improve wear resistance in the engine contact conjunctions. Wear prevention does not necessarily improve fuel efficiency [32]. Dahotre and Nayak [33] suggested that nano-size coating grains can alleviate concerns with respect to coatings' dimensional stability, amenability to honing, residual stresses and hot hardness. They showed that Ni-, MoS_2- and graphite-based coatings have good lubricating properties, whilst Al_2O_3- and SiC-based materials can improve wear resistance of surfaces [33]. Nickel nanocomposite (NNC) is an in-situ mixture of wear-resistant and lubricous particulate within an electroplated nickel matrix. NNC is used to improve tribological behaviour of cylinder bores in racing applications [32]. Diamond-like carbon (DLC) coatings tolerate large substrate stresses under extreme EHL contacts such as in cam-tappet pairs [32]. NNC is studied in this paper due to its similarity with Ni-SiC, a brand largely used by manufacturers of advanced cylinder liners for motorsport engines because of its low friction characteristics. Automotive companies dealing with high performance engines are also interested in wear resistant DLC cylinder liners if the compromise on frictional losses is deemed as marginal. Reports associated with the application of DLC in cylinder bores are largely contradictory. Rejowski et al [34] reported a 2.5% friction reduction using DLC, whilst Sato et al [35] observed negligible frictional improvements. Nevertheless, the effect of coatings on fuel economy and emission levels of IC engines has not hitherto been reported in a fundamental predictive manner, which is one of the original contributions of the current study.

Coating technology is an innovative approach in mitigating the environmental impacts of IC engines. This paper strives to model and predict the effect of coating materials on the global fuel economy and emission of the vehicle fleet. Study of tribology and thermal behaviour of coated engine components assists with the understanding of the breadth of such an impact. The current study focuses only on a single piston ring-cylinder bore conjunction. A rigid piezo-viscous contact model is developed, which captures heat flows from the contiguous component surfaces onto the compression ring. A thermal network analysis is carried out, based on the approach of Morris et al [19]. However, the modified thermal model in the current study accounts for the topography and thermal conductivity of the coating layer as well, which is another original contribution of the current study. Gas pressure applied behind the piston ring is predicted using a blow-by model, based on the approach of Namazian and Heywood [36]. The blow-by analysis is not detailed in this paper for the sake of brevity. Fuel consumption for the nominated bore surfaces is estimated using the relationship between the theoretical power loss and the air-fuel ratio

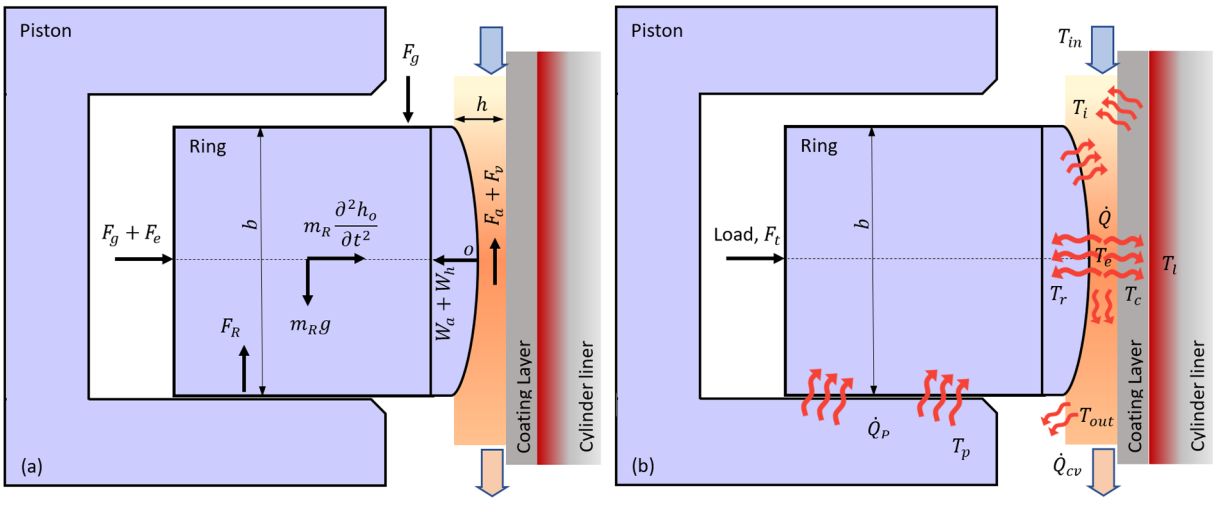

Fig. 1. Schematics of piston ring – cylinder bore conjunction: (a) tribodynamic model and (b) thermal model.

(AFR) [37]. CO emission has a simple empirical relationship with AFR and equivalence in spark ignition (SI) engines [38]. Thus, CO emission is utilised to qualitatively represent the trend in CO_2 emission during dynamometric testing.

This paper investigates the implication of coating technology on fuel economy and emissions, incorporating multi-scale, multi-physics modelling of ring dynamics, contact tribology, thermal effects and gas blow-by. The original contributions of the current research are: (i) analytical prediction of the effect of coating materials on tribological and thermal behaviour of piston compression ring conjunction with advanced cylinder liners for high performance and motorsport applications, and (ii) extrapolated environmental impact of in-service advanced coating technology on the global vehicle fleet fuel economy and emissions. The current analysis is confined to the study of the piston compression ring-cylinder liner conjunction of a modified Honda CRF 450R motocross motorsport engine, which incorporates a compression ring and an oil control ring. The study does not include the frictional performance of piston skirt.

2. Methodological outline

A single-cylinder, four-stroke Honda CRF450 motocross motorsport SI engine is used in the current study. This engine allows for extreme operating conditions found in modern high-performance engines despite being naturally aspirated and equipped with a carburettor. Swanson [39] experimentally compared the brake specific CO emission and fuel consumption of carburettor and fuel injection systems. He showed that carburettor-equipped SI engines can produce power and fuel efficiencies comparable to direct injection engines with negligible differences in their CO emissions [39]. To enable various bore surface coatings to be tested, the engine cylinder block is modified to accept changeable cylinder bore inserts.

Fig. 1 shows schematically the dynamic, tribological and thermal loads of the top compression ring. The analysis comprises rigid-body dynamics of the ring and a one-dimensional (1D) tribological model with appropriate rheological functions. Gas pressure applied behind the inner rim of the piston ring is determined through a gas blow-by model. A one-dimensional Reynolds equation suffices in order to describe the lubricated contacts with peripheral bore-to-ring contact width ratio exceeding 30 [40]. Thermal film shear thinning effect increases the probability of direct interaction of opposing surface asperities. A thermal network model based on the concept of a control volume is deployed to estimate the temperatures of the lubricant and the contiguous rough contacting surfaces (Fig. 1b). The fuel mass flow rate through the intake valve is described using an isentropic compressible flow through a flow restriction. Power loss fluctuations are investigated for the nominated (alternative) bore surfaces. The predicted fluctuations are related to fuel energy and emissions through appropriate theoretical and empirical models. Finally, the environmental impact of coating technology is extrapolated to the global vehicle fleet.

2.1. Tribology and dynamics of compression ring

Pressure distribution and lubricant film thickness are evaluated using one-dimensional Reynolds equation [41] with squeeze film effect, which takes into account the transient conditions.

$$\frac{\partial}{\partial x}\left[\frac{\rho h^3}{6\eta}\left(\frac{\partial p}{\partial x}\right)\right] = U\frac{\partial(\rho h)}{\partial x} + 2\frac{\partial(\rho h)}{\partial t} \tag{1}$$

It is assumed that there is no side leakage of the lubricant in the circumferential direction of the bore. This is reasonable due to generally starved boundary conditions. Furthermore, ring rotation about the bore axis is considered as negligible [37]. The ring velocity, U, is the same as the primary sliding velocity of the piston, $\dot{x}_p$ [42]:

$$U = \dot{x}_p = r\omega\sin\theta + \frac{\omega\cos\theta[c_{cs} + r\sin\theta]}{\sqrt{l^2 - (c_{cs} + r\sin\theta)^2}} \tag{2}$$

where r, l, θ, ω and c_{cs} are crank radius, connecting-rod length, angular position of the crankshaft, its angular velocity and the crankshaft offset respectively. Inlet and outlet pressures are determined through a blow-by model, based upon the work of Namazian and Heywood [36]. This model accounts for ring rigid body dynamics inside its retaining piston groove. Lubricant density variation with pressure and temperature is evaluated using modified Dowson and Higginson relationship [43]:

$$\rho = \rho_o\left[1 + \frac{0.6\times10^{-9}(p - p_o)}{1 + 1.7\times10^{-9}(p - p_o)}\right][1 - 0.65\times10^{-3}(T_e - T_o)] \tag{3}$$

where T_e is the average lubricant temperature inside contact. Viscosity variations with contact pressure and temperature can be predicted using Houpert's equation [44]:

$$\eta(p,\ T_e) = \eta_o\exp\left\{(\ln\eta_o + 9.67)\left[\left(\frac{T_e - 138}{T_o - 138}\right)^{\frac{\beta_o(T_o-138)}{\ln\eta_o+9.76}}\left(1 + \frac{p - p_o}{1.98\times10^8}\right)^{\frac{1.98\times10^8\alpha_o}{\ln\eta_o+9.76}} - 1\right]\right\} \tag{4}$$

The lubricant film thickness (shape) is given as:

$$h(x,\ t) = h_m(t) + S(x) \tag{5}$$

where h_m and $S(x)$ are the minimum film thickness and piston ring face-width axial profile respectively. Localised deformation of the ring is neglected due to the relatively low contact pressures in this partially conforming contact (of the order of a few MPa) [14,19]. The Honda CRF450 piston compression ring in the current study is made of nitrided steel with a titanium-nitride (TiN) coating on its contact face-width. The ring face axial profiles is measured at various locations using the Alicona infinite focus microscope with a nominal vertical resolution of 10 nm and 50x objective. A 6th order polynomial is fitted to the averaged ring face axial profile (Fig. 2):

$$S(x) = 1.06\times10^{14}x^6 + 6.43\times10^{9}x^5 - 3.2\times10^{6}x^4 + 1.38\times10^{3}x^3 + 16.2x^2 - 5.99\times10^{-4}x \tag{6}$$

The units of x and $S(x)$ are in metres. The contact load can be partly supported by a thin film of lubricant and partly by the direct contact of surface asperities on the opposing counter faces (the regime of lubrication is mostly mixed). The asperity interactions are significant for determining the Stribeck's oil film thickness ratios: $\lambda = h/\sigma < 4.0$, where σ is the composite RMS asperity height of contacting pairs [45]. The ring face axial profile is discretised for the calculation of generated pressures. Thus, the load carried by the asperities is obtained at each discretised element as [20]:

$$\mathrm{d}W_a = \frac{16\sqrt{2}}{15}\pi(\eta_a\beta\sigma)^2\sqrt{\frac{\sigma}{\beta}}E^*F_{5/2}(\lambda_i)\mathrm{d}A \tag{7}$$

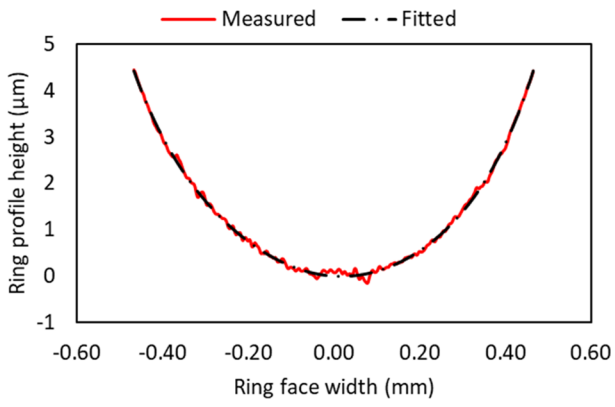

Fig. 2. Measured ring face axial profile and its polynomial curve-fit.

where η_a, β, A, E^*, and λ_i are the number of asperities per unit area, average radius of curvature of asperity peaks, the apparent contact area, reduced Young's modulus of elasticity and the local film thickness ratio respectively. The asperity contact area in each discretised element is obtained as [20]:

$$dA_a = \pi^2(\eta_a\beta\sigma)^2F_2(\lambda_i)dA \tag{8}$$

The surfaces of plateau-honed cylinder bore and its piston ring counterpart follow a Gaussian asperity height distribution after the culmination of the running-in wear. Subsequently, their topography does not alter significantly [46]. The statistical functions $F_2(\lambda)$ and $F_{5/2}(\lambda)$ correlate the real contact area and pressure to the compliance and Gaussian height distribution of the micro-conjunctions of the asperities [45]. The statistical functions are usually approximated using polynomial curve-fits for ease of computation with the drawback of reduced accuracy for larger values of λ [46]. The primitive integral (anti-derivative) of an exponential function equates to another exponential function based on the fundamental theorem of calculus. Hence, an exponential curve-fit can represent the statistical functions more accurately and also ensures computational simplicity. Eqs. (9) and (10) are curve-fits to the indicated values in appendix 2 of Greenwood and Tripp [45], thus:

$$F_2(\lambda) = 3.585\exp\left(-\frac{(\lambda + 2.495)^2}{2\times 1.257^2}\right) \tag{9}$$

$$F_{5/2}(\lambda) = 6.879\exp\left(-\frac{(\lambda + 2.791)^2}{2\times 1.271^2}\right) \tag{10}$$

Thus, the total load carrying capacity at the piston ring – cylinder bore interface is calculated as:

$$W_t = \int_{-b/2}^{b/2}(dW_a + p dA) \tag{11}$$

Greenwood and Tripp [45] contact model is applicable to the elastic deformation of asperities of rough contacting surfaces. This model excludes the adhesion between surface asperities described by the more complex models such as those of Johnson-Kendall-Roberts (JKR) or Derjaguin-Muller-Toporov (DMT). Piston ring velocity, particularly for high performance vehicles is very high during engine strokes and only very momentarily comes to rest at the top and bottom dead centres. Therefore, asperities on the opposing contacting surfaces do not interact for sufficiently long period of time to form adhesive junctions. Therefore, the Greenwood and Tripp elastic contact model [45] deemed to be sufficient for the analysis of boundary friction at piston ring – cylinder liner conjunction. The ring tension is induced through fitment of an incomplete circular elastic ring into the cylinder bore. Chamber gas pressure loading also occurs behind the inner rim of the fitted compression ring. Both these forces push the ring onto the surface of the cylinder bore [20]:

$$F_t = F_e + F_g = \frac{L_g EI}{3\pi b R_{bore}^4} + 2\pi b R_{bore} p_g \tag{12}$$

where L_g, E, I and p_g are the ring free end-gap, Young's modulus of elasticity, second area moment of inertia of ring's cross-section and gas pressure behind the ring. The viscous shear stress acting on the bore surface is calculated along the contact interface as:

$$\tau_v = -\eta(p, T)\frac{U}{h} - \frac{h}{2}\left(\frac{dp}{dx}\right) \tag{13}$$

Thus, the viscous friction can be predicted as:

$$f_v = \int_{-b/2}^{b/2}|\tau_v|\, dA_v, \quad \text{where} \quad dA_v = dA - dA_a \tag{14}$$

A thin film of lubricant separates the asperity tips during their direct interactions. Eyring shear stress, τ_o, determines the shear threshold for non-Newtonian behaviour of the lubricant. The pressure coefficient of boundary shear stress of the asperities, ξ, is measured using atomic force microscopy (AFM) in lateral force mode (LFM). The boundary lubrication contribution to total friction is evaluated as [20]:

$$f_b = \int_{-b/2}^{b/2}(\tau_o dA_a + \xi dW_a) \tag{15}$$

The total friction, f_f, becomes:

$$f_f = f_v + f_b \tag{16}$$

and the power loss is [47,48]:

$$P_l = \int_{-b/2}^{b/2}\left[\eta(p, T)\frac{U^2}{h} + \frac{h^3}{12\eta(p, T)}\left(\frac{dp}{dx}\right)^2\right]dA + f_b U \tag{17}$$

Friction mean effective pressure (FMEP) is obtained for an engine cycle as [37]:

$$fmep = \frac{\bar{P}_l n_R}{V_d N} \tag{18}$$

where n_R is the number of crank revolutions per engine cycle. N represents the crankshaft revolutions per second and the mean power loss, $\bar{P}_l$, is averaged over an engine cycle. The swept volume by the piston, V_d, is expressed in cubic metres as [37]:

$$V_d = \pi R_{bore}^2(2r) \tag{19}$$

Reynolds Eq. (1) is solved numerically using finite difference technique. The ring face profile is discretised into 100 intervals and finite differences utilised to implement partial differentiation with respect to the space variable. Pressure convergence is achieved through an iterative solution approach when the pressure convergence criterion: $\varepsilon_p = \frac{|\sum p - p_o|}{\sum p} \le 10^{-4}$ is satisfied, where p and p_o refer to pressures at the current and the previous iteration steps respectively. Contact load convergence is also sought with the error tolerance: $\varepsilon_W = \frac{|F_t - W_t|}{W_t} \le 10^{-3}$. The effect of pressure and film variations on the ring rigid-body dynamics is also taken into account. Dynamic state variables (velocity and displacement) are determined using the Newmark integration method.

2.2. Thermal analysis

Morris et al [19] developed an iterative thermal network model to predict the temperature of entrained lubricant through the contact as well as those of the contacting surfaces themselves. Their study focused on the generated frictional heat in the contact, neglecting any external heat sources. They also disregarded the effect of conductivity of any surface coatings. The current analysis accounts for the generated combustion heat flow through the crevices between the piston ring and its retaining piston grooves. The effect of bore surface coating is also taken into account, which affects the conductive heat transfer away from the contact (Fig. 3). The generated heat, $\dot{Q}$, is considered to be the result of all the frictional power losses in the contact:

$$\dot{Q} = P_l \tag{20}$$

This heat is partly carried away through lubricant convection, $\dot{Q}_{cv}$, and partly by conduction through the piston ring coated surface, $\dot{Q}_r$ and the cylinder bore coated surface, $\dot{Q}_c$. Therefore:

$$\dot{Q} = \dot{Q}_r + \dot{Q}_c + \dot{Q}_{cv} \tag{21}$$

The convective heat flow rate is evaluated as:

$$\dot{Q}_{cv} = \dot{m}_l c_p(T_e - T_i) \tag{22}$$

where $\dot{m}_l = \rho A_c U$ represents the mass flow rate through the minimum gap between the ring and the cylinder bore (minimum film thickness). A_c, c_p and T_e are the cross-sectional area normal to the lubricant flow, specific heat of the lubricant at constant pressure, and the effective lubricant temperature in the conjunction respectively. Assuming that the piston ring is stationary and the cylinder bore represents the moving

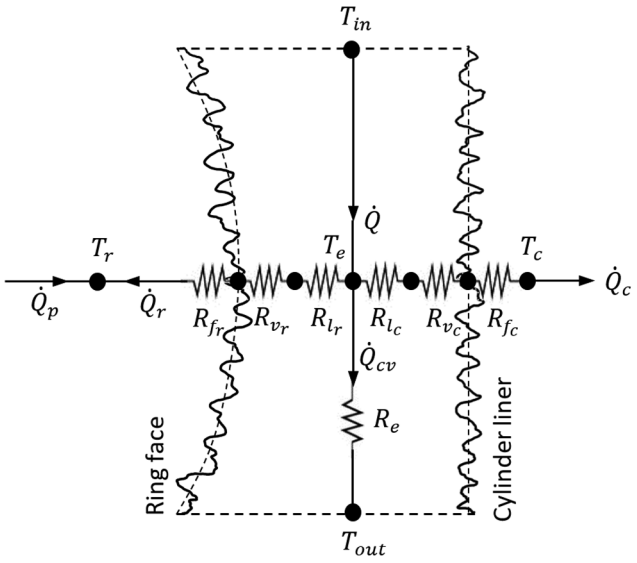

Fig. 3. Schematic of the thermal network model for heat transfer paths within the contact (not to scale).

Table 1
Engine data.

Parameter	Value	Unit
Crank radius	31.05	mm
Connecting rod length	107.00	mm
Crankshaft offset to the anti-thrust side	7.50	mm
Bore nominal diameter	95.92	mm
Ring face-width (axial width)	1.15	mm
Ring thickness (radial width)	3.50	mm
Ring free end-gap	14.50	mm
Intake valve stem diameter, D_s	5.475–5.490	mm
Intake valve guide inner diameter, D	5.500–5.512	mm
Intake valve seat width, w/cosβ	1.1–1.3	mm
Intake valve seat angle, β	45	°
Intake valve head diameter, D_v	25.05	mm

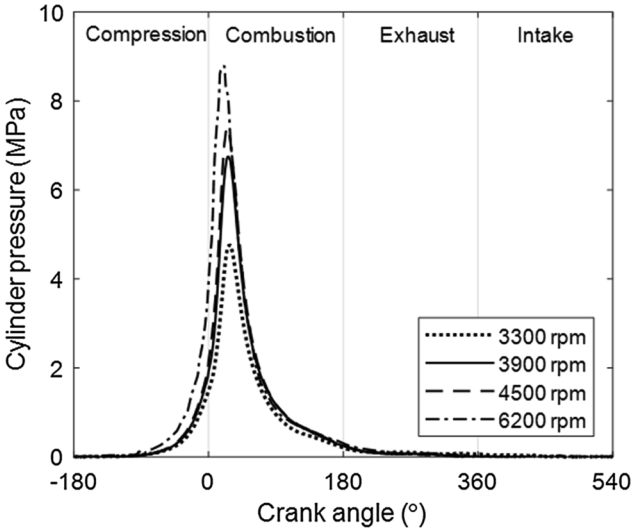

Fig. 4. Measured cylinder pressure variations with crank angle and engine speed.

part, then the lubricant temperature at the inlet equates the cylinder bore coating temperature [12,19]. This assumption is justified considering the heat flux from the cylinder surface prior to the inlet conjunction (Fig. 1a):

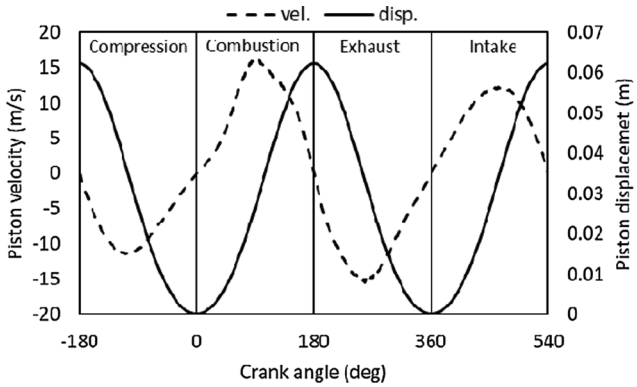

Fig. 5. Piston primary motion kinematics at 3500 rpm: (a) displacement (zero indicates the top dead centre) and (b) piston velocity.

Table 2
Mechanical/thermal properties of piston ring: substrate material and the coating layer [54].

Parameter	Piston ring Fe	Ring coating TiN	Unit
Young's modulus of elasticity	200	251	GPa
Poisson's ratio	0.31	0.25	–
Density	7874	5220	Kg m^{-3}
Thermal conductivity	47–80	19.2	Wm^{-1} K^{-1}
Specific heat capacity	450	484.9	J kg^{-1} K^{-1}
Coating thickness	–	1.5–3	μm

Table 3
Thermo-mechanical properties of the cylinder bore: substrate material and three alternative coatings [24,54,57–58].

Parameter	Cylinder Bore	Bore coatings		Unit
	Steel	DLC	NNC	
Young's modulus of elasticity	200	210	165	GPa
Poisson's ratio	0.31	0.22	0.31	–
Density	7850	3510	5175	Kg m^{-3}
Thermal conductivity	34.3	4.5	42.1	Wm^{-1} K^{-1}
Specific heat capacity	520	1300	566	J kg^{-1} K^{-1}
Coating thickness	–	2.0	50.0–70.0	μm

$$T_{in} = T_i = \frac{T_r U_r + T_c U_c}{U_r + U_c} \approx T_c \tag{23}$$

where the subscripts r and c refer to the ring and the coated cylinder bore surfaces. The generated heat flows through a series of thermal resistive barriers. These barriers are: (i) conduction through the lubricant film, R_l, (ii) convection through the lubricant boundary layer adjacent to the contacting surfaces, R_v, and (iii) the flash temperature of the coated surfaces, R_f.

$$R_l = \frac{h_m}{2k_l A}$$
$$R_v = \frac{1}{h_t A}$$
$$R_{fi} = \frac{S_{fi}}{k_i A} \qquad (i = r, c) \tag{24}$$

where k_l, k_c and k_r are the thermal conductivities of the lubricant, the coated cylinder bore and the coated piston ring. The convective heat transfer coefficient, h_t, at the boundary layer can be predicted, assuming a laminar flow through the conjunction ($h_t = \mathrm{Nu}k_l/h_m$). The characteristic lengths S_{fc} and S_{fr} are determined for the cylinder bore and ring coated surfaces [19] as:

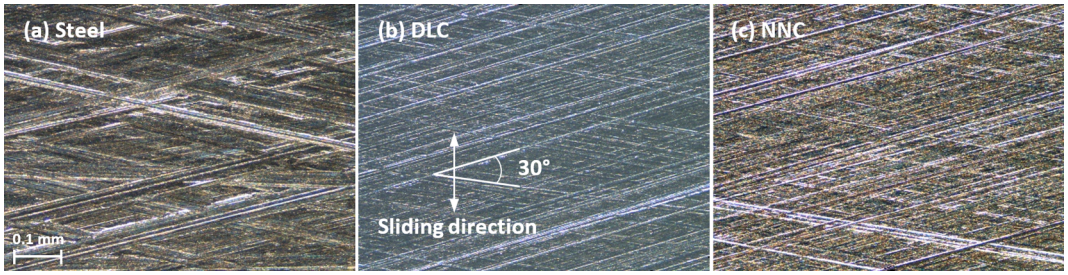

Fig. 6. Plateau-honed Cylinder bores with 30° crosshatch angle: (a) Steel, (b) DLC and (c) NNC.

Table 4
Surface topography of the ring and the bore with and without coating.

Parameter	Ring Surface	Bore surface			Unit
	TiN	Steel	DLC	NNC	
Root mean square height, S_q	0.201	0.482	0.565	0.349	μm
Kurtosis, S_{ku}	3.424	3.240	2.900	3.685	–
Skewness, S_{sk}	−0.283	0.062	0.025	−0.019	–
Density of peaks, S_{pd}	2536	2574	3110	2879	mm^{-2}
Arithmetic mean peak curvature, S_{pc}	0.053	0.227	0.294	0.202	μm^{-1}
Pressure coefficient of boundary shear, ξ	–	0.170	0.219	0.149	–

Table 5
Lubricant rheological parameters [19].

Parameter	Value	Unit
Density	849.7 @15 °C, 833.8 @40 °C	Kg m^{-3}
Kinematic Viscosity	59.99 @40 °C, 9.59 @100 °C	$\times 10^{-6}$ m^2 s^{-1}
Thermal conductivity	0.225 @120 °C	Wm^{-1} K^{-1}
Specific heat capacity	2360 @120 °C	J kg^{-1} K^{-1}
Thermal expansion coefficient	6.5×10^{-4}	K^{-1}

$$S_{fc} = \sqrt{\frac{2k_c b}{\rho_c c_c U}}$$
$$S_{fr} = \frac{1}{\pi A}\left[L^2 b \operatorname{asinh}\left(\frac{b}{L}\right) + Lb^2 \operatorname{asinh}\left(\frac{L}{b}\right) + \frac{1}{3}[L^3 + b^3 - (b^2 + L^2)^{3/2}]\right] \quad (25)$$

where ρ_c and c_c are the density and specific heat for the cylinder bore coating. The bore perimeter is: $L = 2\pi R_{bore}$. The effective thermal resistance for each surface equates to: $R_i = R_l + R_v + R_{fi}$ $(i = r, c)$. The thermal resistance barrier due to convective lubricant flow is: $R_e = 1/\dot{m}_l c_p$. Thus, the lubricant temperature can be obtained as:

$$T_e = \frac{(P_l R_l + T_i)R_c R_r + R_l(R_c T_r + R_r T_c)}{R_c R_r + R_l(R_c + R_r)} \quad (26)$$

The temperature of the piston rises through two distinct mechanisms: (i) heat due to friction, and (ii) heat generated by combustion. The rise in the piston ring temperature is predicted using:

$$\Delta T_r = \frac{R_{fr}}{R_r}(T_e - T_r) + \dot{Q}_p \quad (27)$$

Combustion heat flows through the piston to the piston ring as $\dot{Q}_p$:

$$\dot{Q}_p = \frac{1}{h_{t,pr} A_s}(T_p - T_r) \quad (28)$$

where T_p and T_r are the piston and the compression ring surface coating temperatures respectively. $h_{t,pr}$ is the convective heat transfer coefficient of the lubricant film between the ring and its retaining groove. The contact area in this conjunction is A_s. The cylinder bore temperature for the Honda CRF450 engine was measured near its internal surface using thermocouples [49]. This temperature stabilises after 85 s for various fixed loads and speeds. The speed-averaged temperature is assumed as the surface coating temperature at the bore substrate-coating interface (Fig. 1b).

2.3. Fuel energy efficiency

The mass flow rate through the intake valves can be predicted using a simple orifice model [37,50]. This model neglects the pressure waves occurring inside the inlet and outlet pipes due to any abrupt expansive or compressive flows [51]. However, the fuel mass fluctuations can be approximated as:

$$\begin{cases} \dot{m} = \frac{C_D A_R p_o}{\sqrt{R_s T_o}}\left(\frac{p_T}{p_o}\right)^{1/\gamma}\sqrt{\frac{2\gamma}{\gamma-1}\left[1 - \left(\frac{p_T}{p_o}\right)^{\gamma-1/\gamma}\right]}, & \frac{p_T}{p_o} > \left[\frac{2}{\gamma+1}\right]^{\gamma/(\gamma-1)} \\ \dot{m} = \frac{C_D A_R p_o}{\sqrt{R T_o}}\gamma^{1/2}\left(\frac{2}{\gamma+1}\right)^{\gamma+1/2(\gamma-1)}, & \frac{p_T}{p_o} \le \left[\frac{2}{\gamma+1}\right]^{\gamma/(\gamma-1)} \end{cases} \quad (29)$$

The temperature of the fuel mixture at the inlet valve, T_o, can be approximated as the cylinder head temperature. Representative temperatures have been measured and reported in the open literature [9,37,52]. The cylinder pressure, p_T, falls below atmosphere when the intake valve opens [37,51]. The upstream pressure wave, p_o, at the intake manifold is approximately twice the cylinder pressure during the intake [51]. Specific heat ratio, γ, is considered to be 1.4. The coefficient of discharge and the ratio of valve head diameter to average valve lift are considered to be $C_D = 0.55$ and $L_v/D_v = 0.2$ [50] respectively. The reference area, A_R, is the characteristic of valve design and equals the intake valve curtain area [37]:

$$A_R = \pi D_v L_v \quad (30)$$

The stoichiometric AFR is evaluated for a known fuel chemical formulation using [37]:

$$\left(\frac{A}{F}\right)_{\text{stoich}} = \frac{35.56(4+y)}{12.011 + 1.008y}, \quad \text{where } y = \frac{b}{a},\ C_aH_b \quad (31)$$

The chemical formulation for gasoline is C_8H_{15} [50]. The actual AFR was read from the lambda sensor in an engine test cell for the Honda CRF450 with $(A/F)_{\text{actual}} = 12$. The mass flow rate of air-fuel mixture is known from Eq. (29). Thus, the fuel mass flow rate can be predicted using the actual definition of AFR as:

$$\dot{m}_f = \frac{\dot{m}}{(A/F)_{\text{actual}} + 1} \quad (32)$$

The intake valve opens about 10–25 degrees before the top dead centre (TDC) and closes 30–70 degrees after the bottom dead centre (BDC). The available fuel mass in the combustion chamber can be estimated using the intake valve timing, Δt_{IVO}, at various engine speeds. Thus, the fuel energy available is:

$$E_{in} = m_f Q_{LHV} \quad (33)$$

where the lower heating value of fuel: $Q_{LHV} \approx 45$ MJ/kg. Effective output energy, E_{eff}, equals $E_{in} - (E_{loss} + \delta E_{loss})$. Energy loss for uncoated cylinder surface, E_{loss}, is utilised as a reference and any variations from this value, δE_{loss}, are due to the coating characteristics. For a fixed

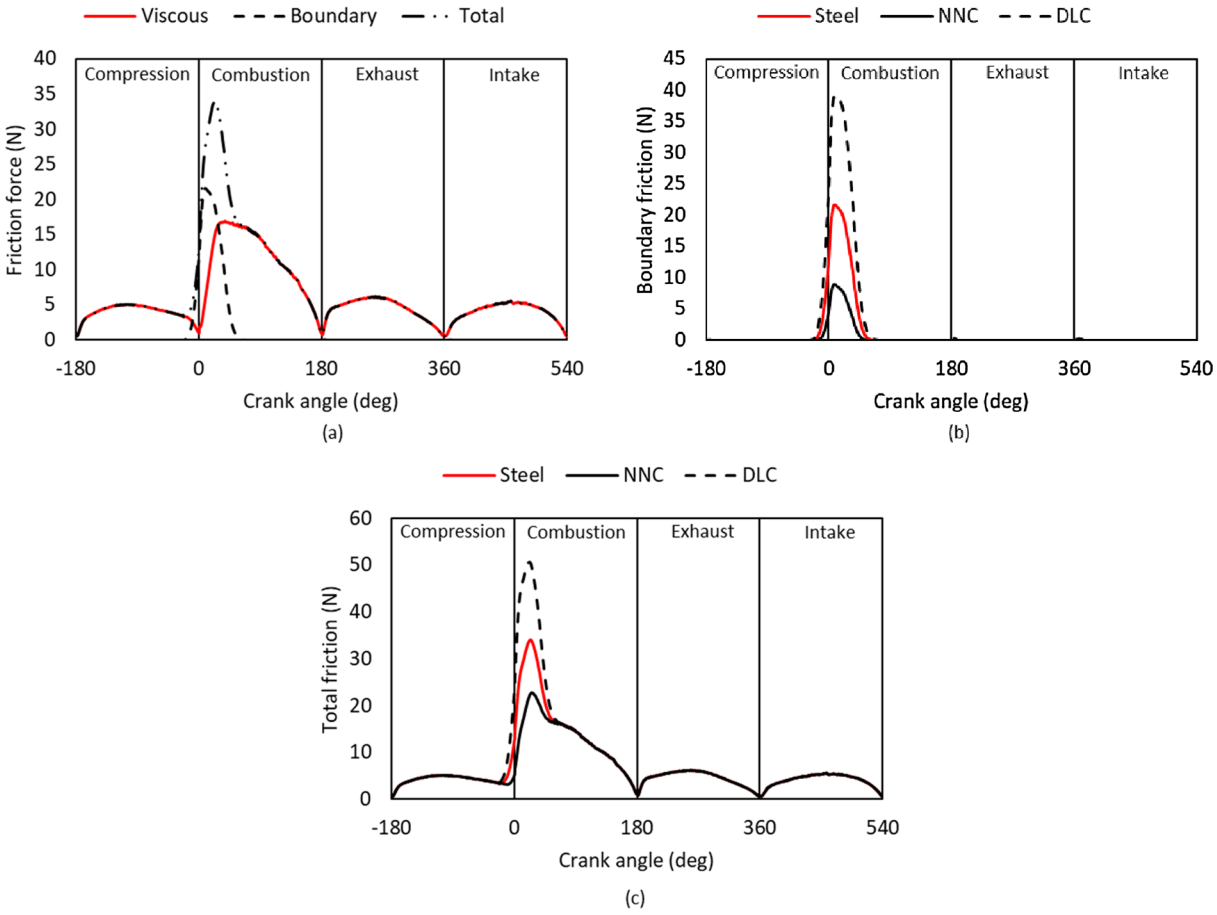

Fig. 7. Frictional variation with crank angle for (a) TiN-Steel conjunction, (b) boundary friction for different cylinder bore surfaces and (c) total friction for different cylinder surfaces at 3500 rpm.

effective output energy, the fuel mass varies with the energy loss fluctuations: $\delta m_f = \delta E_{loss}/Q_{LHV}$. The variations in energy loss are predicted using the power loss fluctuations during an engine cycle [16] as:

$$\delta E_{loss} = \int_0^{t_{cycle}} \delta P_l \mathrm{d}t = \delta P_{ave} \cdot \Delta t \tag{34}$$

The emissions increase proportional to the excess fuel mass. A simple empirical relationship is established between the CO emission and the equivalence ratio, ϕ, for spark ignition (SI) engines [38]. CO_2 is the by-product of CO, following the oxidisation reaction ($CO + OH = CO_2 + H$). Thus, calculated CO values can be considered as representative of CO_2 emission for coated cylinder bores. The equivalence ratio is:

$$\phi = \frac{(A/F)_{\text{stoich}}}{(A/F)_{\text{actual}}} \tag{35}$$

where $(A/F)_{\text{actual}}$ includes the effect of fuel mass variation, δm_f. The following relationship is the CO emission index for SI engines [38]:

$$\text{EI}_{\text{CO}} = \begin{cases} \exp(-8.395 + 5.518\phi^2), & \phi < 1 \\ -2.725 + 2.78\phi, & \phi \geq 1 \end{cases} \tag{36}$$

3. Results and discussion

Table 1 lists the specifications of the single-cylinder, four-stroke Honda CRF450 SI engine used in the current study. The standard cast cylinder block was replaced with a wet block design, comprising a holder block and a cylinder bore. This modification was essential to simplify the removal of cylinder liners and reduce the cost of experimentation [46]. Despite being naturally aspirated, this engine produces representative side forces due to the relatively large bore compared with the more contemporary small-bore turbo-charged engines. Cylinder pressures were measured under fired engine dynamometric tests using a spark plug-type Kistler pressure transducer for a range of speeds: 3000–6500 rpm (Fig. 4) [53] at 50–75% throttle. Cylinder pressures at other engine speeds are interpolated using Lagrangian polynomial interpolation. Appendix A describes the uncertainties in measurements of all input data such as cylinder pressure, crank-angle and surface roughness. For the sake of brevity, friction and thermal studies are detailed only for a single engine speed of 3500 rpm. Fuel energy and emissions are investigated in a dynamometric test at average speeds representative of a standard World-wide harmonised Light-vehicle Test Cycle (WLTC). Fig. 5 shows the piston primary motion kinematics, using Eq. (2). Angular position and angular velocity of the crankshaft are the main inputs to Eq. (2). These parameters are measured from engine dynamometry. Piston velocity can reach 15 m/s in mid-strokes at 3500 rpm.

Tables 2 and 3 provide the specifications of the mechanical and thermal properties of the piston compression ring, cylinder bore and their coating layers. The coating properties in Ref. [54] are provided by the manufacturer for the same coated cylinder liners in this study. The piston ring is coated with titanium nitride (TiN) to harden and protect its surface in sliding motion. A standard steel uncoated cylinder bore and two bores with nickel nanocomposite (NNC) and diamond-like carbon (DLC) bore coatings are used in the current study. The cylinder bores are plateau honed at approximately 30° crosshatch angle (Fig. 6). The manufacturing process produces crosshatched grooves which serve as reservoirs of lubricant. This optimal angle has been verified through various statistical, analytical and experimental studies [24,55–56].

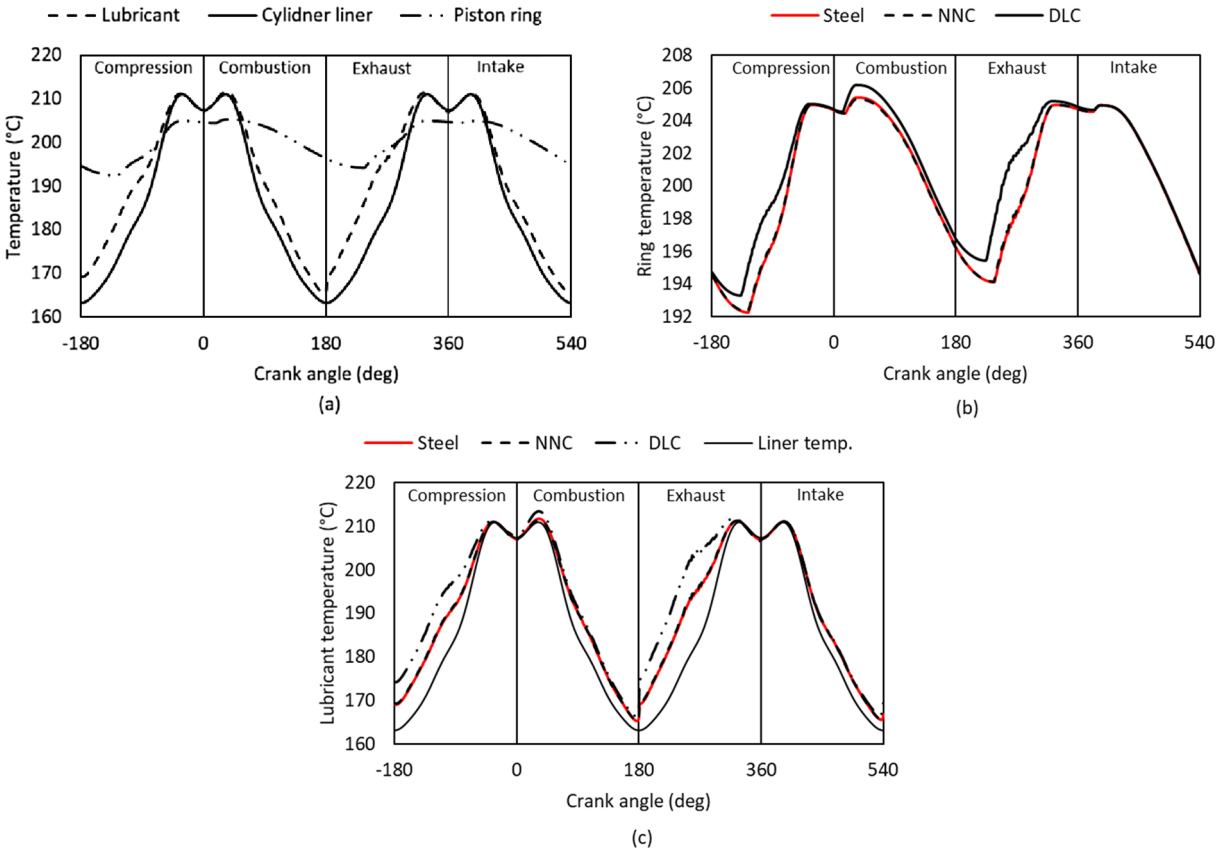

Fig. 8. Temperature variation for (a) TiN-steel lubricated conjunction, (b) piston ring surface against alterative cylinder bore coatings and (c) lubricant medium at nominated conjunctions during an engine cycle at 3500 rpm and ¾ load (base bore temperature).

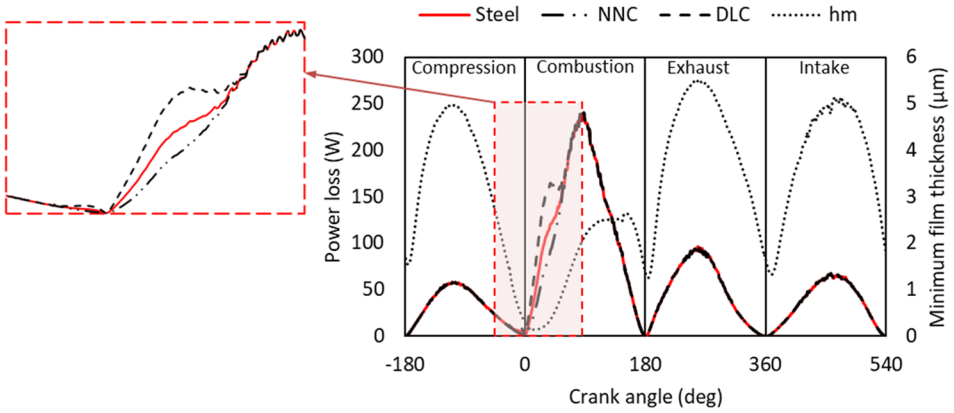

Fig. 9. Power loss and the variation in the minimum film thickness, h_m, with various cylinder bore coating material during an engine cycle at 3500 rpm.

Surface roughness parameters were measured at several locations on the piston ring and cylinder bores using white light interferometry with 50x magnification factor (Table 4). The pressure coefficient of boundary shear, ξ, of the real rough surfaces was measured for the cylinder bore surfaces using an Atomic Force Microscope (AFM) operating in Lateral Force Mode (LFM). Non-conductive silicon nitride tips with 19–20 nm radii were employed. The test atmosphere was controlled at the temperature of 20 ± 0.5 °C and relative humidity of 50 ± 5%. The experiments were carried out over a 1 μm^2 area with 1 μm/sec tip velocity. Further details on the measurement of friction using AFM and associated data analysis procedures can be found in [18,54]. The measured values are listed in Table 4. The uncertainty in the measurement of surface topography is also determined in Appendix A. Table 5 provides the rheological properties of the lubricant at the reference temperatures. The effective density and viscosity values are predicted at the operating temperatures using Eqs. (3) and (4).

The combined tribological and thermal performance of the alternative bore surface coatings are analysed in this study. The methodology adapted in this study has already been validated in [20,59,60]. The results for the uncoated surface are used as the baseline for ascertaining the performance of the coated cylinder bores. Frictional variations with crank angle are shown for the uncoated steel cylinder bore in Fig. 7a. The piston compression ring conjunction with the cylinder bore undergoes hydrodynamic regime of lubrication for a large part of the engine cycle. Hence, viscous shear is the main mechanism of friction generation for much of the engine cycle. The gas pressure acting behind the inner rim of the piston compression ring rises in the vicinity of the top dead centre in the compression and combustion strokes. The lubricant film thickness reduces below the average height of the composite asperity heights of the contacting counter face surfaces in these

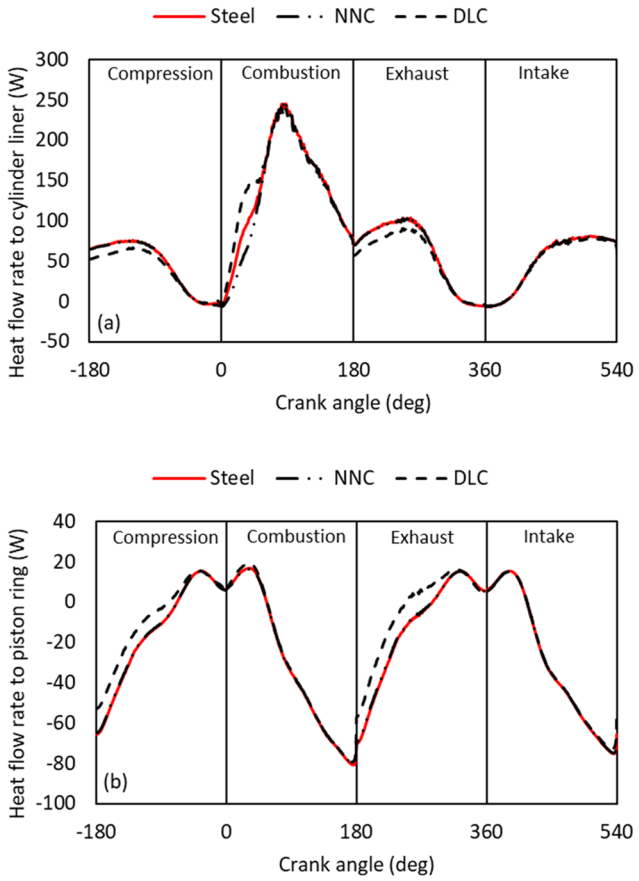

Fig. 10. Thermal losses due to heat flow rate to (a) cylinder bore and (b) piston ring during an engine cycle at 3500 rpm (Positive and negative values indicate flows into and out of the surface, respectively.)

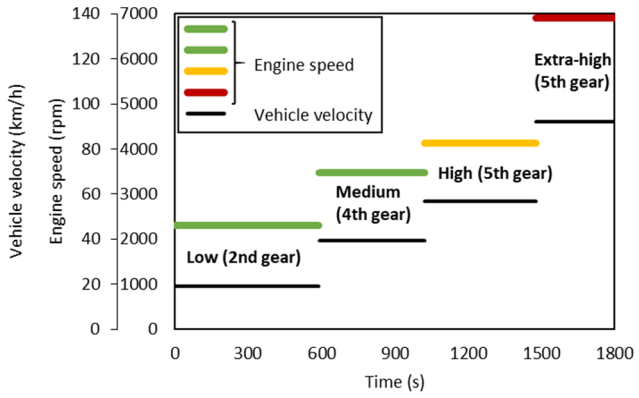

Fig. 11. Considered dynamometric test phases inspired by the WLTC cycle for Honda CRF450 engine (transitions between consecutive phases are treated quasi-statically).

parts of the engine cycle. Consequently, the properties of surface coatings significantly affect boundary friction (Fig. 7b) and heat transfer. These issues have not hitherto been considered in previously reported analyses in the open literature. The DLC coating performs quite poorly during the mixed regime of lubrication as the friction increases by 20 N in comparison with the standard steel cylinder bore (the baseline surface). This increase is partly due to the poor thermal conductivity of the DLC (Table 3) and partly due to its high pressure coefficient of boundary shear (Table 4). Note that the DLC is essentially a good wear-resistant coating, but has high adhesion because of its relatively smooth topography. DLC has been shown to effectively

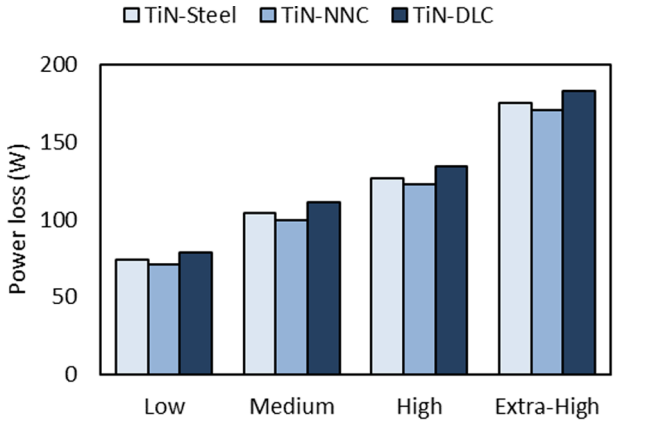

Fig. 12. Mean power loss for alternative cylinder bores in an engine cycle at speeds representative of dynamometric test phases.

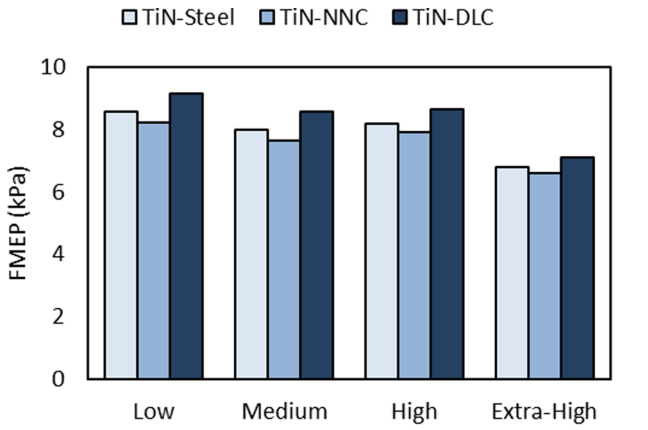

Fig. 13. FMEP for the various alternative cylinder bores during the period of dynamometric test phases.

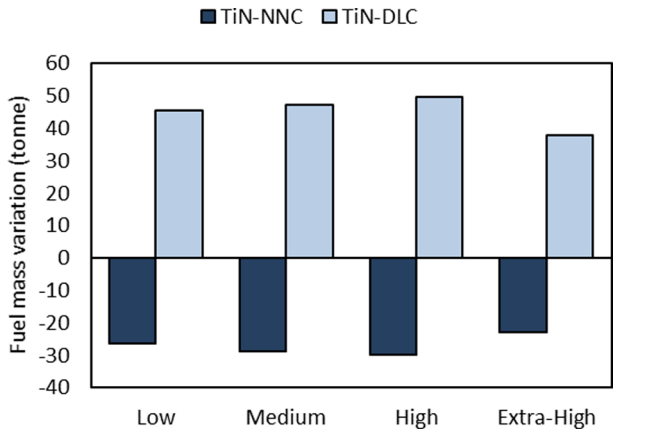

Fig. 14. Estimated potential fuel mass change per cylinder of the global gasoline vehicle fleet (1 billion vehicles with gasoline engines by 2040) based on dynamometric test phases (zero represents the uncoated steel cylinder bore surface).

improve the tribological performance of high-pressure elastohydrodynamic contacts (> 1 GPa) by preventing the high stresses from penetrating into the substrate material [61]. Contact pressures are relatively low in the partially-conforming compression ring conjunction and the low thermal conductivity of DLC increases the contact temperature.

Lubricant film shear thinning with temperature exacerbates boundary friction. NNC coating reduces the boundary friction by less

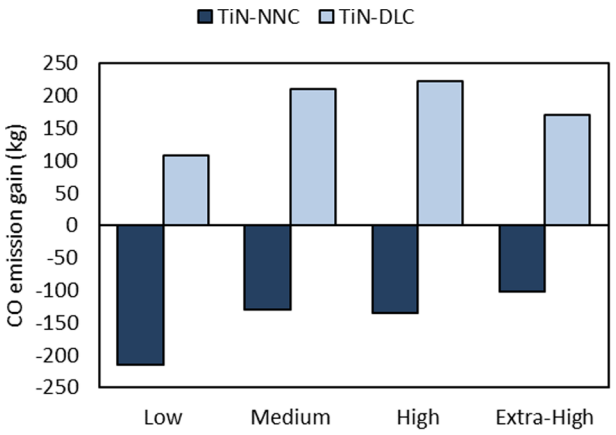

Fig. 15. Estimated potential CO emission change per cylinder of the global vehicle fleet with gasoline engines (1 billion gasoline vehicles by 2040) based on dynamometric test phases (zero represents the uncoated steel cylinder bore surface).

than 10 N (Fig. 7b). The pressure coefficient of boundary shear is low for this surface owing to reduced adhesion (Table 4). Its thermal conductivity is higher than steel (Table 3). Fig. 7c shows the combined effects of viscous and boundary friction contributions during an engine cycle.

The measured cylinder bore temperature is utilised in the thermal analysis (Fig. 8a). The bore temperature stabilises after 85 s for various load-speed combinations [48]. Thus, the stroke-to-stroke temperature variations is neglected in the current analysis. The predicted lubricant temperature follows the cylinder bore temperature closely, which is in accord with the findings of other researchers [12,19]. Heat transfer from the piston to the piston ring was often neglected in the previous studies. Therefore, the piston ring and lubricant were reported to follow similar temperatures. Fig. 8a shows that the piston ring temperature rises by up to 30 °C above the cylinder bore temperature due to heat transfer from piston groove lands onto it. Heat flow from ring to lubricant reverses near the top dead centre due to high cylinder bore temperature. Here the piston ring temperature rises accordingly. Fig. 8b shows the piston ring temperature variations with different cylinder surfaces. Steel and NNC surfaces manifest similar thermal behaviours, whilst the piston ring temperature rises for the DLC coating. NNC has reduced friction mainly due to its tribological properties. The poor frictional performance of DLC coating is due to its tribological and thermal properties in a simultaneous manner. However, the thermal efficiency of the engine, also comprising thermodynamic combustion heat as well as friction-generated heat, is expected to improve with DLC coating due to less heat being lost from the chamber. Lubricant temperature rises mainly through the conduction mechanism, whilst convection through lubricant remains almost unaltered (Fig. 8c). This is because of the thinness of the lubricant film and generally quite low lubricant flow through the contact conjunction.

The power losses from the coated surfaces deviate from the uncoated steel surface during the combustion stroke (Fig. 9). The film thickness is comparable to the asperity heights during this part of the engine cycle and consequently mixed regime of lubrication is dominant (from −30° to 90° crank angles). The DLC conjunction is prone to a larger power loss due to its higher pressure coefficient of boundary shear and poorer thermal conductivity. The NNC coating produces less friction and therefore shows a relatively better tribological performance than the DLC variant. Fig. 10a and 10b show heat flow rates from the lubricant to the cylinder bore and the piston ring, respectively. Positive values indicate the heat flow from the lubricant into the surfaces and vice versa. The DLC coated cylinder bores better isolate the combustion chamber thermally under transient conditions, but overall this effect can be quite marginal. Therefore, heat flow rate through the DLC coated cylinder bore is lower during the compression and exhaust strokes (Fig. 10a). Thermodynamic efficiency of the engine can thus potentially improve using DLC coatings during the part of the cycle with dominant hydrodynamic regime of lubrication. Fig. 10b shows that the combustion heat flows through the piston ring to the lubricant (i.e. negative values – however, this can become marginal on the basis of mean surface temperature with respect to that of the combustion chamber temperature). Thus, lubricant convection is responsible for the cooling of the contact. This trend reverses during the combustion stroke where direct asperity interactions are prevalent. Boundary friction is larger for the DLC coating and also more friction heat is generated. Therefore, the temperature gradient between the lubricant and the cylinder bore increases.

Simultaneously, contact thermal resistance reduces for thin lubricant films. Therefore, heat flow rate through the DLC coating is enhanced relative to that for the uncoated steel surface (Fig. 10a). This temperature gradient is smaller for the NNC coating and the heat flow rate reduces during the combustion stroke. Therefore, coating technology can significantly affect power loss and thermal efficiency of a single piston ring conjunction. Investigation of its impact on fuel economy and emission is imperative, considering the global vehicle fleet with multi-cylinder IC engines.

Legislative authorities have introduced various emission regulations, backed by specified vehicle/dynamometric test cycles. WLTC is one such cycle. It is a dynamic cycle with realistic driving conditions. It provides an accurate measure of CO emissions of IC engines [62–64]. Replication of this cycle in a numerical analysis is quite time consuming and computationally inefficient. Alternatively, a representative dynamometric test, inspired by the WLTC, is utilised (Fig. 11). It comprises four vehicle speed phases: (i) low speed urban driving in congested traffic (low), (ii) urban medium speed driving (medium), (iii) combined urban and motorway driving (high) and (iv) high speed motorway driving (extra-high). For computational simplicity, the vehicle is assumed to cruise at a constant engine speed and gear (i.e. no gear shifting) during each of these phases. Gear shifting between consecutive phases is also neglected and treated quasi-statically. The cruise speed is determined through the average speed of the vehicle during each phase. Frictional losses are analysed for the indicative speeds and cylinder pressures. With these assumptions, the predictive accuracy is somewhat compromised for the sake of timely computations. With the benefit of hindsight, the predictive accuracy for fuel economy and emission varies within an order of magnitude. Moreover, the current study focuses on the potential gains accrued through use of coating technology available in the global market.

Mean power loss for a single cylinder is calculated for the nominated cylinder bores during an engine cycle at speeds representative of dynamometric test phases and is shown in Fig. 12. The power loss increases with engine speed for these surfaces. Up to 6% power can be potentially saved using the NNC coating relative to an uncoated cylinder bore (Fig. 12). Friction mean effective pressure (FMEP) is a more meaningful measure for engine performance [37]. Mechanical losses at the piston ring conjunction vary with surface type, mainly during the mixed regime of lubrication. Therefore, FMEP is evaluated in transition from the compression stroke to the combustion stroke (i.e. from −30° to 90° crank angle), where the most asperity interactions (boundary lubrication) occurs. The average FMEP for an engine cycle complies with the findings of Regueiro [65]. Predicted FMEP values are extrapolated for the duration of each phase of dynamometric test (Fig. 13). FMEP slightly increases in transition from medium to high speed phases. During extra high speed phase, boundary interactions are at their minimum state, leading to lower FMEP values. This can be attributed to formation of slightly thicker lubricant film, resulting in reduction in the extent of asperity interactions. The NNC coating at this phase performs better in comparison with other surfaces.

A study by Exxon Mobil anticipated over a billion SI engines in the global vehicle fleet by 2040 despite the increasing share of electric-

powered vehicles [2]. Modern engines are equipped with direct injection (DI) nozzles. Honda CRF450 supplies fuel through a carburettor mechanism. Carburettor-equipped SI engines can produce power and fuel efficiency comparable to the DI engines with negligible differences in emissions [39]. Therefore, the findings of this study can be generalised with good approximation. Coating technology potentially improves the engine efficiency at large scale production through the reduction of power losses. Fuel input should proportionally vary with power loss in order to sustain the engine output power (Section 2.3). It should be noted that this study investigates the new bore surfaces and an in-depth study of wear effect is proposed for future research. It is noteworthy that the efficiency and emission analyses presented here are per cylinder of IC engines.

An indicative estimation of the effect of cylinder bore coatings, based on the analysis provided in this study, on reduction from consumed fuel by SI engines can be made on a global scale. In this study, fuel mass and CO emissions are evaluated per cylinder of a typical SI engine during dynamometric test phases. The potential variations per cylinder can be extrapolated to the global vehicle fleet with gasoline engines (~one billion gasoline vehicles by 2040 according to Exxon Mobil). The use of NNC would therefore potentially reduce fuel consumption by 30 tonnes (Fig. 14). In effect, this coating material can control the CO emissions, especially under urban driving conditions (Fig. 15). The predicted values are limited to the top compression ring of a single cylinder SI engine during dynamometric tests (Figs. 14 and 15). The typical useful lifespan of a modern passenger vehicle is approximately 200,000 km [66]. Hence, roughly 760 kilo-tonnes of fuel and 5 kilo-tonnes of CO can be potentially reserved per cylinder of SI engines using coating technology in the global passenger vehicle fleet. Fuel mass saving and reduction of emissions will increase further after accounting for the number of cylinders. Provided that other piston rings (such as second compression) undergo mixed regime of lubrication, the extrapolated gain from coating technology would even be higher.

4. Conclusion

More than 75% of the automotive industry would still rely on IC engines by 2040 in its traditional role, or as a part of a hybrid powertrain or as a range extender. This would be despite a growing trend in the manufacture of electric vehicles. Coating technology, which is currently used mostly in high performance racing vehicles, is an innovative approach to mitigate the environmental impacts of IC engines as advocated in this study for use in the global fleet. A comprehensive multi-scale, multi-physics analytical model of the top compression ring is developed, integrating system and component rigid body dynamics, tribology, thermal effects and gas blow-by. Advanced NNC and DLC coatings are used as alternatives for steel cylinder bore surfaces (a new bore coating). The combustion chamber can be effectively insulated using the DLC coating. However, lubricant performance will be adversely affected by the temperature rise and its load carrying capacity noticeably diminishes in mixed regime of lubrication. The NNC coating improves the tribological performance of the piston ring and reduces the losses due to boundary friction. Similar trends are noted for frictional power loss and FMEP. The analytical study of coating technology for tribological and thermal behaviour of piston ring conjunction is one of the original contributions of the current study. The environmental impact of coating technology on the global fuel economy and emission has not hitherto been reported in literature. An indicative estimation indicated that reductions of 380 kilo-tonnes of fuel and 2.5 kilo-tonnes of CO can be potentially achieved per cylinder of SI engines using the advanced coated cylinder bores over the lifespan of the gasoline powered vehicle fleet. It should be noted that the current analysis neglects the number of cylinders and possible gains which would also be accrued in the other ring conjunctions of typical ring-packs. Cavitation is affected by surface features such as roughness and textures [67]. The proposed methodology can be utilised in the future to analyse the interlinked effect of coatings and cavitation on frictional performance and emissions. Moreover, with progressive hybridisation of future powertrains, IC engines will still be deployed at least for the next few decades as the secondary source of power or as range extenders along with electric power. Downsized IC engines, often operating at non-optimal temperatures would lead to exacerbated frictional losses and emissions. Although the focus of this research is not on hybrid powertrains, the proposed methodology can be applied to investigate the implications of advanced coating materials on the performance of hybrid systems. Finally, future work can include direct measurement of frictional losses and blow-by, affected by alternative surface coatings in controlled dynamometric tests. Floating liner can be used for direct measurement of friction as in Gore et al [68] and blow-by as routinely performed in such tests. Such investigations would help validation of the methodology described here and forms a part of the future direction of the current research.

Declaration of Competing Interest

The authors declare that they have no known competing financial interests or personal relationships that could have appeared to influence the work reported in this paper.

Acknowledgements

The authors would like to express their gratitude to Capricorn Automotive Ltd. for its technical and financial support and to the Engineering and Physical Sciences Research Council (EPSRC) for its financial support under the Doctoral Training Program (DTP). Capricorn Automotive Ltd. was involved in experimental tasks and the development of this manuscript.

Appendix A

Experimental measurements are potentially subjected to two sources of error, including systematic (fixed) and random errors. The former is reduced through careful calibration. The uncertainty due to random errors can be predicted statistically. Uncertainty of a measured parameter x_R, can be evaluated using:

$$\Delta x_R = \frac{1.96\sigma_R}{x_{R,m}} \tag{A.1}$$

where $x_{R,m}$ and σ_R are the mean value and standard deviation of the measured parameter, x_R, successively. The total uncertainty, U_t, is the root mean square (RMS) of the uncertainties due to systematic error, E_{sys}, and random error, Δx_R, i.e.

$$U_t = \sqrt{(\Delta x_R)^2 + (E_{sys})^2} \tag{A.2}$$

Some of the measured parameters are inputs to the analytical model. The uncertainties associated with the measured parameters x_i ($i = 1, 2, \cdots$) are Δx_i. The uncertainty in a calculated function G_f will be $G_f \pm \Delta G_f$ if the system parameters are linearly correlated and ΔG_f can be evaluated as [69]:

Table A.1
Total uncertainty in measured parameters.

Measured parameter	Sensor Manufacturer	Model	Range	Systematic error E_{sys}	Random error Δx_R	Total Uncertainty U_t
Crank angle	Hubner Berlin	TTL 1024	360 pulse/rev	0.03%	0.28%	0.28%
Cylinder pressure	Kistler	6081A40	0–250 bar	0.80%	0.78%	1.12%
Surface Roughness	Alicona	Infinite Focus	0.02–1.19 μm	2.00%	1.60%	2.56%

Table A.2
Power loss and FMEP uncertainties.

Input Parameter	Input uncertainty (%)	Output uncertainty (%)	
		Power loss	FMEP
Crank angle	± 0.280	± 0.000	± 0.000
Cylinder pressure	± 1.120	± 0.675	± 0.674
Surface Roughness	± 2.560	± 0.311	± 0.311
Combined analysis (Total)	–	± 0.985	± 0.986

$$\frac{\Delta G_f}{G_f} = \sqrt{\left(\frac{\Delta x_1}{x_1}\frac{\partial G_f}{\partial x_1}\right)^2 + \left(\frac{\Delta x_2}{x_2}\frac{\partial G_f}{\partial x_2}\right)^2 + \cdots} \tag{A.3}$$

In the current study, the model parameters are nonlinearly dependent, and the covariance between them is not easily calculated. Therefore, the uncertainty thresholds for power loss and FMEP analyses are directly evaluated using the error margins reported in Table A.1. The input uncertainties are used in the numerical model at 6900 rpm. At this speed, pressure and crank angle errors are at their maximum. Table A.2 shows the uncertainties of power loss and FMEP considering individual and combined errors in the measured parameters.

References

[1] Bayindir KÇ, Gözüküçük MA, Teke A. A comprehensive overview of hybrid electric vehicle: Powertrain configurations, powertrain control techniques and electronic control units. Energy Convers Manage 2011;52(2):1305–13.
[2] Report: 2017 Outlook for Energy: a view to 2040. Exxon Mobil Corporation; 2017. Accessed online on May 2019 at: https://cdn.exxonmobil.com/~/media/global/files/outlook-for-energy/2017/2017-outlook-for-energy.pdf.
[3] Abdel-Rahman AA. On the emissions from internal-combustion engines: a review. Int J Energy Res 1998;22(6):483–513.
[4] Roberts A, Brooks R, Shipway P. Internal combustion engine cold-start efficiency: a review of the problem, causes and potential solutions. Energy Convers Manage 2014;82:327–50.
[5] Demirbas A. Political, economic and environmental impacts of biofuels: a review. Appl Energy 2009;86:S108–17.
[6] Enomoto Y, Furuhama S, Minakami K. Heat loss to combustion chamber wall of 4-Stroke gasoline engine: 1st report, heat loss to piston and cylinder. Bull JSME 1985;28(238):647–55.
[7] Rahnejat H. Tribology and dynamics of engine and powertrain: fundamentals, applications and future trends. Cambridge, UK: Woodhead Publishing; 2010.
[8] Richardson DE. Review of power cylinder friction for diesel engines. J Eng Gas Turb Power 2000;122(4):506–19.
[9] Furuhama S, Tada T, Nakamura T. Some measurements of the piston temperatures in a small type gasoline engine. Bull JSME 1964;7(26):422–9.
[10] Mierbach A, Dück GE Newman BA. Heat flow through piston rings and its influence on shape. SAE Technical Paper, No. 831283; 1983.
[11] Ma MT, Sherrington I, Smith EH. Analysis of lubrication and friction for a complete piston-ring pack with an improved oil availability model: Part 1: circumferentially uniform film. Proc IMechE Part J: J Eng Tribol 1997;211(1):1–15.
[12] Ma Z, Henein NA, Bryzik W. A model for wear and friction in cylinder bores and piston rings. Tribol Trans 2006;49(3):315–27.
[13] Priest M, Dowson D, Taylor CM. Predictive wear modelling of lubricated piston rings in a diesel engine. Wear 1999;231(1):89–101.
[14] Mishra PC, Balakrishnan S, Rahnejat H. Tribology of compression ring-to-cylinder contact at reversal. Proc IMechE, Part J: J Eng Tribol 2008;222(7):815–26.
[15] Mishra PC. Tribodynamic modelling of piston compression ring and cylinder bore conjunction in high-pressure zone of engine cycle. Int J Adv Manuf Technol 2013;66(5–8):1075–85.
[16] Rahmani R, Theodossiades S, Rahnejat H, Fitzsimons B. Transient elastohydrodynamic lubrication of rough new or worn piston compression ring conjunction with an out-of-round cylinder bore. Proc IMechE, Part J: J Eng Tribol 2012;226(4):284–305.
[17] Baker C, Theodossiades S, Rahmani R, Rahnejat H, Fitzsimons B. On the transient three-dimensional tribodynamics of internal combustion engine top compression ring. J Eng Gas Turb Power 2017;139(6):062801.
[18] Styles G, Rahmani R, Rahnejat H, Fitzsimons B. In-cycle and life-time friction transience in piston ring–bore conjunction under mixed regime of lubrication. Int J Engine Res 2014;15(7):862–76.
[19] Morris N, Rahmani R, Rahnejat H, King PD, Fitzsimons B. Tribology of piston compression ring conjunction under transient thermal mixed regime of lubrication. Tribol Int 2013;59:248–58.
[20] Rahmani R, Rahnejat H, Fitzsimons B, Dowson D. The effect of cylinder bore operating temperature on frictional loss and engine emissions in piston ring conjunction. Appl Energy 2017;191:568–81.
[21] Morris N, Mohammadpour M, Rahmani R, Johns-Rahnejat PM, Rahnejat H, Dowson D. Effect of cylinder deactivation on tribological performance of piston compression ring and connecting rod bearing. Tribol Int 2018;120:243–54.
[22] Saidur R, Rezaei M, Muzammil WK, Hassan MH, Paria S, Hasanuzzaman M. Technologies to recover exhaust heat from internal combustion engines. Renew Sustain Energy Rev 2012;16(8):5649–59.
[23] He M, Zhang X, Zeng K, Gao K. A combined thermodynamic cycle used for waste heat recovery of internal combustion engine. Energy 2011;36(12):6821–9.
[24] Tomanik E. Modelling the hydrodynamic support of cylinder bore and piston rings with laser textured surfaces. Tribol Int 2013;59:90–6.
[25] Liu Z, Meng X, Wen C, Yu S, Zhou Z. On the oil-gas-solid mixed bearing between compression ring and cylinder liner under starved lubrication and high boundary pressures. Tribol Int 2019;140:105869.
[26] Howell-Smith S. Tribological optimisation of the internal combustion engine piston to bore conjunction through surface modification PhD Thesis Loughborough, UK: Loughborough University; 2010
[27] Gu C, Meng X, Zhang D. Analysis of the coated and textured ring/liner conjunction based on a thermal mixed lubrication model. Friction 2018;6(4):420–31.
[28] Grabon W, Koszela W, Pawlus P, Ochwat S. Improving tribological behaviour of piston ring–cylinder bore frictional pair by bore surface texturing. Tribol Int 2013;61:102–8.
[29] Pawlus P, Cieslak T, Mathia T. The study of cylinder bore plateau honing process. J Mater Process Technol 2009;209(20):6078–86.
[30] Roensch MM. Piston-ring coatings and their effect on ring and bore wear. SAE Trans 1940:221–8.
[31] Jackson JE, Wear-resistant coatings of diesel cylinder bores. SAE Technical Paper, No. 410085; 1941.
[32] Howell-Smith S, Rahnejat H, King PD, Dowson D. Reducing in-cylinder parasitic losses through surface modification and coating. Proc IMechE, Part D: J Automob Eng 2014;228(4):391–402.
[33] Dahotre NB, Nayak S. Nanocoatings for engine application. Surf Coat Technol 2005;194(1):58–67.
[34] Rejowski ED, Mordente Sr P, Pillis MF Casserly T, Application of DLC coating in cylinder bores for friction reduction. SAE Technical Paper, No. 2012-01-1329; 2012.
[35] Sato O, Takiguchi M, Takayuki A, Seki Y, Fujimura K, Tateishi Y, Improvement of piston lubrication in a diesel engine by means of cylinder surface roughness. SAE technical paper, No. 2004-01-0604; 2004.
[36] Namazian M, Heywood JB. Flow in the piston-cylinder-ring crevices of a spark-ignition engine: effect on hydrocarbon emissions, efficiency and power. SAE Trans 1982:261–88.

[37] Heywood JB. Internal combustion engine fundamentals. 2nd ed. USA: McGraw Hill education; 2018.
[38] Shayler PJ, Chick J, Darnton NJ, Eade D. Generic functions for fuel consumption and engine-out emissions of HC, CO and NO x of spark-ignition engines. Proc IMechE, Part D: J Automob Eng 1999;213(4):365–78.
[39] Swanson M. An emission comparison between a Carburetor and an electronic fuel injection system for utility engines. SAE Technical Paper, No. 911806; 1991.
[40] Haddad SD, Tjan KT. An analytical study of offset piston and crankshaft designs and the effect of oil film on piston slap excitation in a diesel engine. Mech Mach Theory 1995;30(2):271–84.
[41] Reynolds O. On the theory of lubrication and its application to Mr. Beauchamp tower's experiments, including an experimental determination of the viscosity of olive oil. Philosoph Trans Roy Soc London 1886;177:157–234.
[42] Rahnejat H. Multi-body dynamics: vehicles, machines, and mechanisms. Bury St Edmunds, UK: Professional engineering Publishing; 1998.
[43] Yang P, Cui J, Jin ZM, Dowson D. Transient elastohydrodynamic analysis of elliptical contacts. Part 2: thermal and Newtonian lubricant solution. Proc Instit Mech Eng, Part J: J Eng Tribol 2005;219(3):187–200.
[44] Houpert L. New results of traction force calculations in elastohydrodynamic contacts. J Tribol 1985;107(2):241–5.
[45] Greenwood JA, Tripp JH. The contact of two nominally flat rough surfaces. Proc Instit Mech Eng 1970;185(1):625–33.
[46] Gore M, Morris N, Rahmani R, Rahnejat H, King PD, Howell-Smith S. A combined analytical-experimental investigation of friction in cylinder bore inserts under mixed and boundary regimes of lubrication. Lubr Sci 2017;29(5):293–316.
[47] Stachowiak GW, Batchelor AW. Engineering Tribology. Amsterdam, Netherlands: Elsevier; 2014.
[48] Booker JF. Basic equations for fluid films with variable properties. ASME J Tribol 1989;111(3):475–83.
[49] Littlefair B. A tribo-dynamic solution for the flexible piston skirt and bore conjunction PhD Thesis Loughborough University; 2013
[50] Ferguson CR, Kirkpatrick AT. Internal combustion engines: Applied thermosciences. 2nd ed. USA: John Wiley & Sons Inc.; 2001.
[51] Gordon BP. Design and simulation of four-stroke engines. Warrendale, P.A., USA: Society of Automotive Engineers; 1999.
[52] Anderson MK, Assanis DN, Filipi ZS. First and second law analyses of a naturally-aspirated, Miller cycle, SI engine with late intake valve closure. SAE Trans 1998:1355–70.
[53] Dolatabadi N, Theodossiades S, Rothberg SJ. On the identification of piston slap events in internal combustion engines using tribodynamic analysis. Mech Syst Sig Process 2015;58:308–24.
[54] Umer J, Morris N, Leighton M, Rahmani R, Howell-Smith S, Wild R, et al. Asperity level tribological investigation of automotive bore material and coatings. Tribol Int 2018;117:131–40.
[55] Michail SK, Barber GC. The effects of roughness on piston ring lubrication—Part II: the relationship between cylinder wall surface topography and oil film thickness. Tribol Trans 1995;38(1):173–7.
[56] Spencer A, Almqvist A, Larsson R. A numerical model to investigate the effect of honing angle on the hydrodynamic lubrication between a combustion engine piston ring and cylinder bore. Proc Instit Mech Eng Part J: J Eng Tribol 2011;225(7):683–9.
[57] Humphrey E, Morris NJ, Rahmani R, Rahnejat H. Multiscale boundary frictional performance of diamond like carbon coatings. Tribol Int 2018. https://doi.org/10.1016/j.triboint.2018.12.039.
[58] Woolman J, Mottram RA. The mechanical and physical properties of the British standard En steels, volume 3, En40 to En363. Oxford, UK: British Iron and Steel Research Association, Pergamon Press; 1968.
[59] Gore M, Rahmani R, Rahnejat H, King PD. Assessment of friction from compression ring conjunction of a high-performance internal combustion engine: A combined numerical and experimental study. Proc Instit Mech Eng, Part C: J Mech Eng Sci 2016;230(12):2073–85.
[60] Baker C, Rahmani R, Theodossiades S, Rahnejat H, Fitzsimons B. On the effect of transient in-plane dynamics of the compression ring upon its tribological performance. J Eng Gas Turb Power 2014;137(3):032512.
[61] Teodorescu M, Rahnejat H, Gohar R, Dowson D. Harmonic decomposition analysis of contact mechanics of bonded layered elastic solids. Appl Math Model 2009;33(1):467–85.
[62] Pavlovic J, Marotta A, Ciuffo B. CO2 emissions and energy demands of vehicles tested under the NEDC and the new WLTP type approval test procedures. Appl Energy 2016;177:661–70.
[63] Pavlovic J, Ciuffo B, Fontaras G, Valverde V, Marotta A. How much difference in type-approval CO2 emissions from passenger cars in Europe can be expected from changing to the new test procedure (NEDC vs. WLTP). Transp Res Part A: Policy Pract 2018;111:136–47.
[64] Marotta A, Pavlovic J, Ciuffo B, Serra S, Fontaras G. Gaseous emissions from light-duty vehicles: moving from NEDC to the new WLTP test procedure. Environ Sci Technol 2015;49(14):8315–22.
[65] Regueiro A, Daimler Chrysler's New 1.6 L, Multi-Valve 4-Cylinder Engine Series. SAE Technical Paper. No. 2001-01-0330; 2001.
[66] Castro MB, Remmerswaal JA, Reuter MA. Life cycle impact assessment of the average passenger vehicle in the Netherlands. Int J Life Cycle Assess 2003;8(5):297–304.
[67] Gu C, Meng X, Xie Y, Zhang D. Mixed lubrication problems in the presence of textures: an efficient solution to the cavitation problem with consideration of roughness effects. Tribol Int 2016;103:516–28.
[68] Gore M, Theaker M, Howell-Smith S, Rahnejat H, King PD. Direct measurement of piston friction of internal-combustion engines using the floating-liner principle. Proc IMechE, Part D: J Automob Eng 2014;228(3):344–54.
[69] Holman JP. Experimental methods for engineers. 7th ed. London, UK: McGraw-Hill; 2001.